Journal of Medicinal Chemistry

ACS AuthorChoice

Article

pubs.acs.org/jmc

Terms of Use

Structural–Functional Studies of *Burkholderia cenocepacia* D-Glycero-β-D-manno-heptose 7-Phosphate Kinase (HldA) and Characterization of Inhibitors with Antibiotic Adjuvant and Antivirulence Properties

Ting-Wai Lee,[†,#] Theodore B. Verhey,[†,#] Pavel A. Antiperovitch,[†] Dmytro Atamanyuk,[‡] Nicolas Desroy,[‡,∞] Chrystelle Oliveira,[‡] Alexis Denis,[‡,×] Vincent Gerusz,[‡] Elodie Drocourt,[‡] Slade A. Loutet,[§,●] Mohamad A. Hamad,[§] Christian Stanetty,[∥] Sara N. Andres,[†] Seiji Sugiman-Marangos,[†] Paul Kosma,[∥] Miguel A. Valvano,[§,⊥] Francois Moreau,[‡] and Murray S. Junop*[,†]

[†]Department of Biochemistry and Biomedical Sciences and Michael G. DeGroote Institute for Infectious Disease Research, McMaster University, 1280 Main Street West, Hamilton, Ontario, L8S 4K1, Canada

[‡]MUTABILIS, 102 Avenue Gaston Roussel, 93230 Romainville, France

[§]Centre for Human Immunology, Department of Microbiology and Immunology, Western University, London, Ontario, N6A 5C1, Canada

[∥]Department of Chemistry, University of Natural Resources and Life Sciences, Muthgasse 18, A-1190 Vienna, Austria

[⊥]Centre for Infection and Immunity, Queen's University of Belfast, Belfast BT9 7BL, United Kingdom

Supporting Information

ABSTRACT: As an essential constituent of the outer membrane of Gram-negative bacteria, lipopolysaccharide contributes significantly to virulence and antibiotic resistance. The lipopolysaccharide biosynthetic pathway therefore serves as a promising therapeutic target for antivirulence drugs and antibiotic adjuvants. Here we report the structural–functional studies of D-glycero-β-D-manno-heptose 7-phosphate kinase (HldA), an absolutely conserved enzyme in this pathway, from *Burkholderia cenocepacia*. HldA is structurally similar to members of the PfkB carbohydrate kinase family and appears to catalyze heptose phosphorylation via an in-line mechanism mediated mainly by a conserved aspartate, Asp270. Moreover, we report the structures of HldA in complex with two potent inhibitors in which both inhibitors adopt a folded conformation and occupy the nucleotide-binding sites. Together, these results provide important insight into the mechanism of HldA-catalyzed heptose phosphorylation and necessary information for further development of HldA inhibitors.

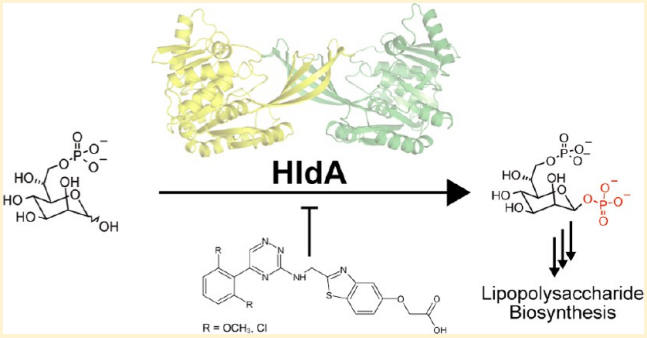

INTRODUCTION

Antibiotic resistance, one of the most pressing problems in the management of infectious diseases, is causing a crisis in the health-care sector. Multidrug resistance (MDR) has been rapidly evolving in bacterial species commonly associated with infections in hospitals and communities, as a consequence of vertical gene transfer within each species and horizontal gene transfer among different species.[1] While MDR in Gram-positive bacteria (e.g., *Staphylococcus aureus*, *Enterococcus faecium*) has been receiving much attention from the pharmaceutical sector, efforts for overcoming that in Gram-negative bacteria (e.g., *Burkholderia cenocepacia*, *Pseudomonas aeruginosa*, *Escherichia coli*) have been limited, despite the fact that many of the latter bacteria are well-known for being among the most common and the most dangerous opportunistic pathogens to immunocompromised individuals such as cystic fibrosis patients and that the efficacy of currently available antibiotics in combating these bacteria has been declining. New therapeutic strategies and new antibiotics are urgently needed in confronting the problem of MDR.[2] A variety of physiological processes in bacteria have been identified as targets for new antibacterial therapeutics; for example, peptidoglycan biosynthesis, drug efflux, and DNA topoisomerization.[3−6]

The defining characteristic of Gram-negative bacteria is the presence of an outer membrane, an asymmetric lipid bilayer whose outer leaflet is mainly composed of lipopolysaccharide (LPS). LPS forms a dense mesh and helps to anchor proteins in the outer membrane. On one hand, this maintains the structural integrity of the outer membrane, which is essential for adhesion to host cells and interaction with host immune effectors including serum components. This implicates LPS as a key virulence factor.[7] On the other hand, the dense hydrophilic mesh of LPS renders the outer membrane impermeable to hydrophobic molecules, which include many currently available antibiotics such

Received: October 12, 2012
Published: December 20, 2012

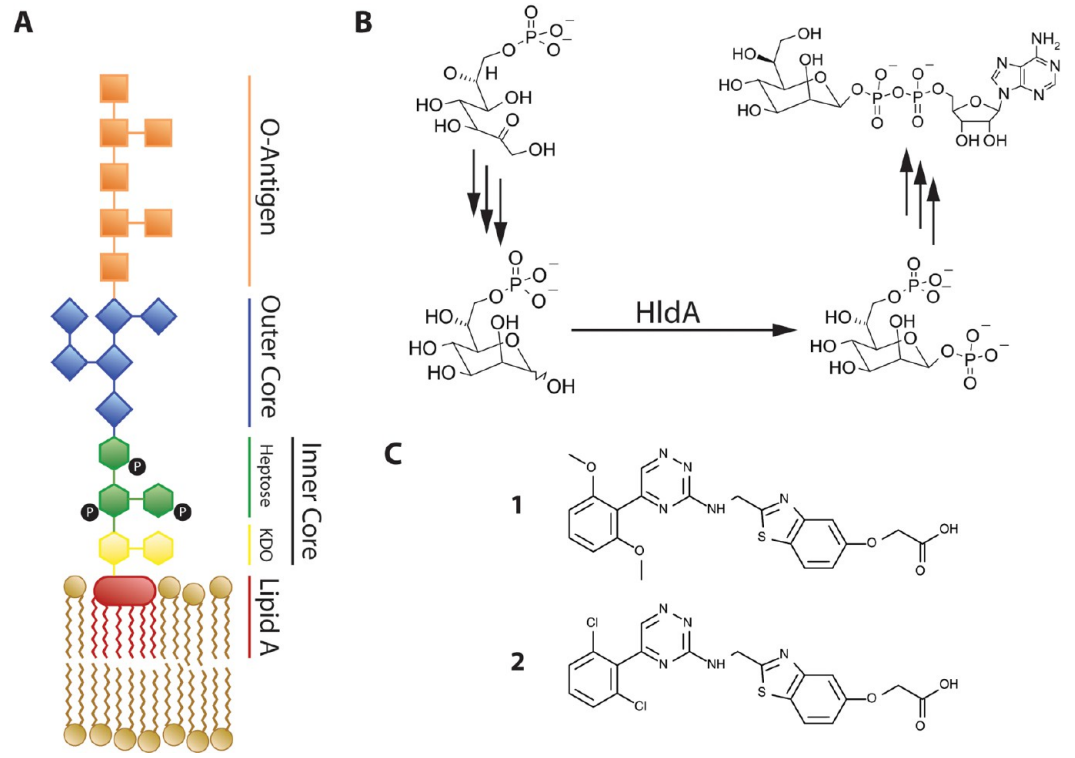

Figure 1. Lipopolysaccharide (LPS). (A) Schematic diagram of the structure of LPS. (B) Biosynthesis of ADP-L-glycero-β-D-manno-heptose, a precursor for the biosynthesis of the inner core region of LPS, from D-sedoheptulose 7-phosphate. The phosphorylation reaction converting D-glycero-β-D-manno-heptose-7-phosphate (M7P) to D-glycero-β-D-manno-heptose-1,7-bisphosphate (GMB) is catalyzed by HldA. (C) Two potent inhibitors of HldA. IC_{50} values against HldA are the following: 0.81 μM for **1**; 0.23 μM for **2**.

as macrolides.[8] LPS comprises lipid A, a core oligosaccharide (OS) and, in some bacterial species, an O-antigen polysaccharide chain. The core OS can be further divided into an inner core region consisting of 2-keto-3-deoxy-D-manno-octosonic acid (KDO) and heptose (prevalently L-α-D-manno-heptose) residues and an outer core region consisting mostly of hexose residues (Figure 1A).[9,10] Lipid A and KDO are indispensable for cell viability and conserved in virtually all Gram-negative bacteria.[11] Their biosynthetic pathways have become targets for the development of traditional antibiotics.[12,13] Interestingly, mutant cells with minimal LPS (i.e., LPS comprising lipid A and KDO only) are viable but display the so-called deep-rough phenotype. In particular, they exhibit increased sensitivity to hydrophobic molecules owing to the lack of negatively charged groups in the truncated LPS for cross-linking by divalent cations, which disfavors the formation of a dense mesh in the outer membrane. In most species, these negatively charged groups are contributed by phosphorylated heptose residues.[11]

ADP-L-glycero-β-D-manno-heptose is a precursor for the biosynthesis of the inner core region of LPS. The pentose phosphate pathway supplies D-sedoheptulose 7-phosphate, which is converted to ADP-L-glycero-β-D-manno-heptose in five steps. Specifically, the second step is a phosphorylation reaction converting D-glycero-β-D-manno-heptose-7-phosphate (M7P) to D-glycero-β-D-manno-heptose 1,7-bisphosphate (GMB), and the fourth step is a nucleotidyl transfer reaction converting D-glycero-β-D-manno-heptose 1-phosphate to ADP-D-glycero-β-D-manno-heptose.[14] In most species (e.g., *E. coli*, *P. aeruginosa*, *Klebsiella pneumonia*), a single bifunctional enzyme, HldE, catalyzes these two steps; but in some others (e.g., *B. cenocepacia*, *Neisseria meningitidis*, *Neisseria gonorrhoeae*), two separate enzymes, HldA and HldC, catalyze the second and the fourth steps, respectively (Figure 1B). HldA and HldC are homologous to the N- and the C-terminal domains of HldE, respectively.[15] Previous studies have shown for some of the ADP-L-glycero-β-D-manno-heptose biosynthetic enzymes that deletion or mutation of their corresponding genes leads to the production of heptoseless LPS, resulting in increased bacterial sensitivity to antibiotics and increased susceptibility to lysis mediated by the host complement.[7,14,16,17]

It is hypothesized that inhibition of the biosynthesis of ADP-L-glycero-β-D-manno-heptose results in the production of defective LPS, thereby increasing the sensitivity of Gram-negative bacteria to host defense and hydrophobic antibiotics. Absent in human cells, this biosynthetic pathway presents a highly advantageous therapeutic target. Inhibitors of ADP-L-glycero-β-D-manno-heptose biosynthetic enzymes can serve as antibiotic adjuvants, coadministered with currently available antibiotics to enhance their efficacies. Alternatively, these inhibitors could be administered alone to prevent infections in immunocompromised patients. To facilitate structure-based inhibitor design, crystal structures have been determined previously for some of the ADP-L-glycero-β-D-manno-heptose biosynthetic enzymes.[18−22] Here, we report four crystal structures of HldA, one showing simultaneously its enzyme−substrate and enzyme−product complexes (ES/EP) and three showing complexes with two potent inhibitors (**1** and **2**, Figure 1C), which were designed using medicinal chemistry from a hit identified by high-throughput screening (that work is reported in the subsequent article, in which inhibitors **1** and **2** are described as compounds **25** and **85**, respectively).[23,24] To our knowledge, these structures are the first ever reported for a heptose kinase, providing valuable insights into the mechanisms of its catalysis and inhibition, which will aid in the development of drugs with antivirulent and membrane-permeabilizing properties.

dx.doi.org/10.1021/jm301483h | J. Med. Chem. 2013, 56, 1405−1417

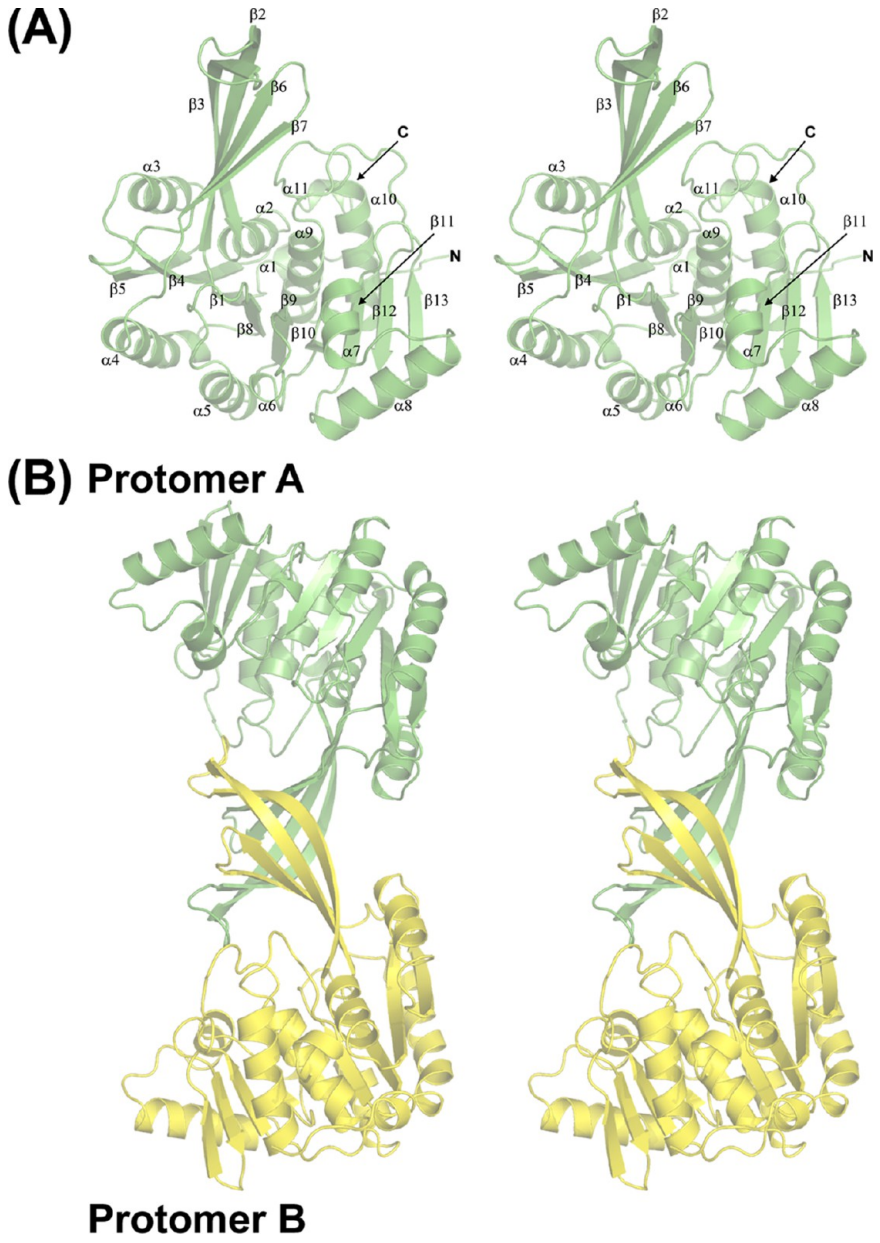

Figure 2. Overall structure of HldA. (A) HldA protomer. The N- and the C-termini and the secondary structure elements are labeled. (B) HldA homodimer. Protomers A and B are shown in green and yellow, respectively.

RESULTS AND DISCUSSION

Crystal Structure of HldA ES/EP (Resolution: 2.60 Å). The amino acid sequence of HldA includes the two signature motifs (the N-terminal Gly-rich motif and the C-terminal GXGD motif) characterizing members of the PfkB carbohydrate kinase family.[25] A search of the Protein Data Bank using the DALI server shows that HldA structurally aligns best with members of the PfkB carbohydrate kinase family (*Z*-scores mostly higher than 20) despite low sequence identities (below 25%).[26] Each protomer of HldA comprises an α/β core and a protruding twisted β-sheet. The α/β core adopts a variant Rossmann fold, with a twisted nine-stranded β-sheet ($\beta5\uparrow\beta4\uparrow\beta1\uparrow\beta8\uparrow\beta9\uparrow\beta10\uparrow\beta11\uparrow\beta12\downarrow\beta13\uparrow$) sandwiched by five α-helices on one face ($\alpha4$, $\alpha5$, $\alpha6$, $\alpha7$, and $\alpha8$) and four α-helices on the opposite face ($\alpha2$, $\alpha3$, $\alpha9$, and $\alpha10$). A short α-helix forms at both the N- ($\alpha1$) and the C-termini ($\alpha11$) of each protomer. $\alpha1$ is located near the N-terminus of $\beta4$ and the C-termini of $\alpha2$ and $\alpha9$, while $\alpha11$ is shielded from the β-sheet in the α/β core by $\alpha2$, $\alpha9$, and $\alpha10$. The protruding twisted β-sheet is composed of four β-strands ($\beta3\downarrow\beta2\uparrow\beta6\uparrow\beta7\downarrow$), with $\beta2$ and $\beta3$ formed in the extended loop connecting $\beta1$ to $\alpha2$, and $\beta6$ and $\beta7$ in that connecting $\beta5$ to $\alpha4$ (Figure 2A). The two protomers in the asymmetric unit are related by noncrystallographic 2-fold symmetry, interacting with each other through their protruding twisted β-sheets. Their protruding twisted β-sheets are oriented orthogonally with respect to each other, and the $\beta3$ of each protomer has its N-terminus bent to form hydrogen bonds with the $\beta7$ of the opposite protomer in a parallel β-sheet fashion. This leads to the formation of a slightly flattened β-barrel with its openings orthogonal to the 2-fold axis (also known as β-clasp, Figure 2B).[27] A total of 2250 Å^2 of solvent-accessible surface area is buried upon dimerization. The dimer interactions are mainly hydrophobic in nature. Importantly, the ζ-guanidinium group of Arg38 at the C-terminus of $\beta2$ of each protomer forms ionic interactions with

dx.doi.org/10.1021/jm301483h | J. Med. Chem. 2013, 56, 1405−1417

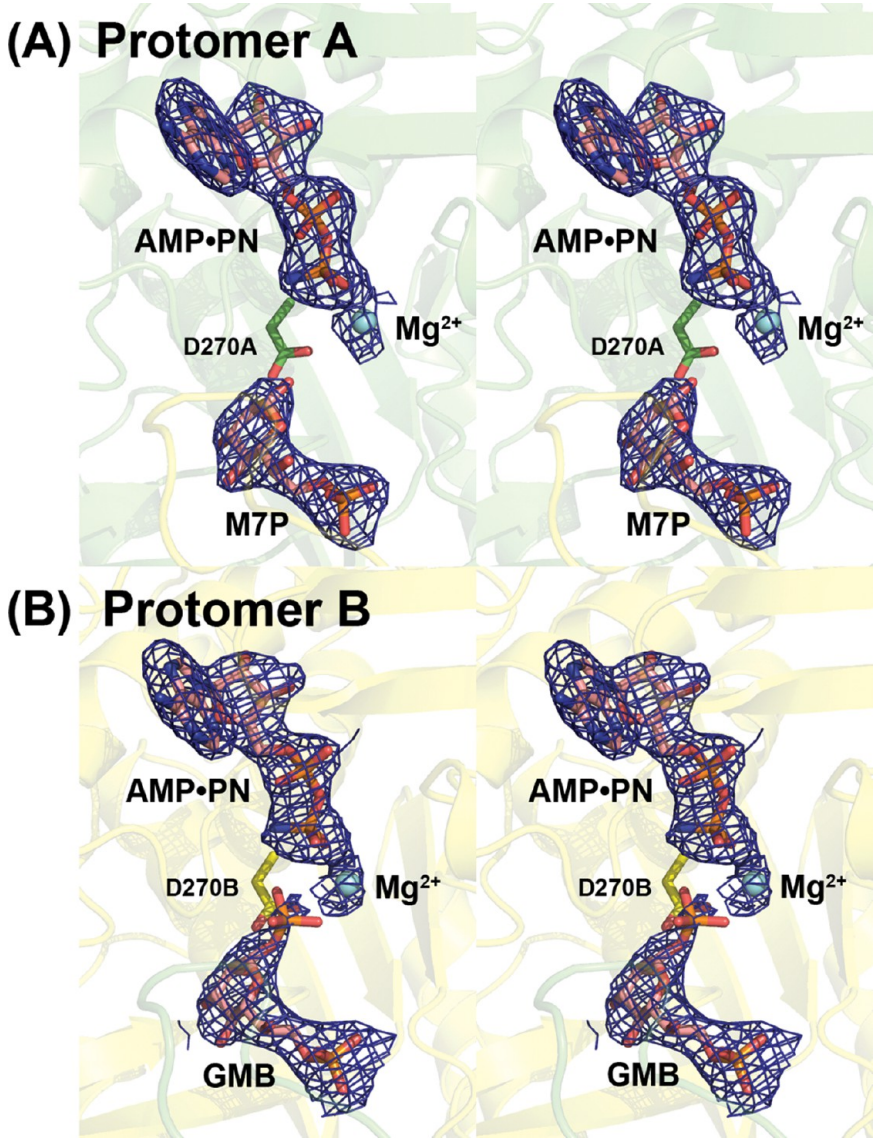

Figure 3. Residual electron densities in the $(2|F_o| - |F_c|)\alpha_c$ map of HldA ES/EP contoured at 1.0σ: (A) active site of protomer A; (B) active site of protomer B. Asp270, AMP·PN, M7P, and GMB are shown with stick models. The magnesium ion is shown in cyan.

the side chain carboxylate groups of Asp127 and Glu129 at the C-terminus of β7 of the opposite protomer, while the δ-carboxylate group of Glu42 in the loop connecting β2 to β3 of each protomer forms ionic interactions with the ζ-guanidinium groups of Arg115 in β6 and Arg125 in β7 of the opposite protomer. Superimposition of the two protomers of HldA (based on main-chain atoms) yielded an rmsd of 0.26 Å, indicating that both protomers adopt essentially the same structure and conformation.

For all of the members of the PfkB carbohydrate kinase family whose three-dimensional structures have been determined so far, the active site is located between the α/β core and the protruding twisted β-sheet of each protomer. Interestingly, at the initial stage of structural model refinement, outstanding electron densities were found between the α/β core and the protruding twisted β-sheet in both protomers of HldA. The shapes and the magnitudes of these electron densities strongly indicate that the hydrolyzed ATP analogue and the substrate of HldA, AMP·PN and M7P, bind in this location of protomer A (Figure 3A), whereas AMP·PN and GMB (the product of HldA) bind in this location of protomer B (Figure 3B). Both M7P and GMB are in the β-pyranose form and in the chair conformation. The GXGD signature motif (Gly267-Ala268-Gly269-Asp270, with Asp270 being putatively central to the catalytic function) forms the N-terminus of α9, located between the nucleotide and the heptose in both protomers.

In both protomers, the nucleotide-binding site is constituted solely by residues from the α/β core. The shapes of the outstanding electron densities clearly indicate that the adenine ring of the nucleotide is in the *syn* orientation, making van der Waals contacts with the main-chain atoms of Ser240 and Glu241 in the loop connecting β11 to β12 and with the side chains of Ala257, Ala259, Val262, and Val265 in the loop connecting β13 to α9 and Val301 at the C-terminus of α10. The ribose ring of the nucleotide is in the C3′-*endo* conformation, with its 2′-hydroxyl group hydrogen-bonded to the γ-amide group of Asn294 in α10 and with its 3′-hydroxyl group hydrogen-bonded to the main-chain carbonyl group of Gly243 at the N-terminus of β12. The negative charges of the phosphate groups of the nucleotide are accommodated by the positive ends of the helix dipoles of α7 and α9, with the N-terminus of α7 in a distance of approximately 6 Å

dx.doi.org/10.1021/jm301483h | *J. Med. Chem.* 2013, 56, 1405−1417

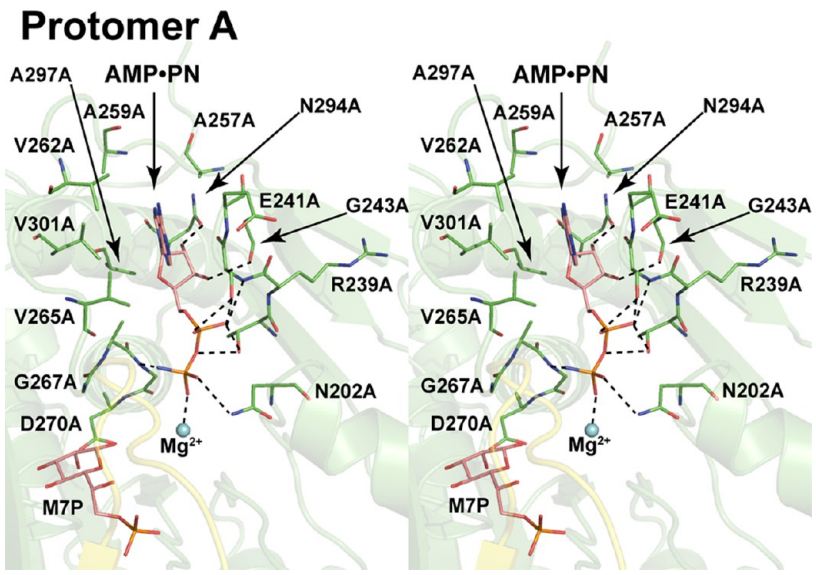

Figure 4. Nucleotide-binding site. Only the site in protomer A is shown, as the nucleotide-binding interactions in protomer B are essentially the same. AMP·PN, M7P, and all of the residues involved are shown with stick models, while the magnesium ion is shown in cyan. For clarity, only some of the residues are labeled. All of the hydrogen bonds involved are indicated by dashed lines.

from both the α- and the β-phosphate groups and with the N-terminus of α9 in a distance of approximately 3.5 Å from the β-phosphate group. The α-phosphate group forms hydrogen bonds through its oxygen atom O1A with the main-chain NH group of Ser240, through O1A and O2A with the γ-hydroxyl group of Ser240, and through O1A and O3A with the γ-hydroxyl group of Thr238 at the C-terminus of β11. The β-phosphate group forms hydrogen bonds through O1B with the γ-amide group of Asn202 at the N-terminus of α7 and through N3B with the main-chain NH group of Gly269. Residues Asn202 to Glu205 constitute the NXXE motif conserved in many members of the PfkB carbohydrate kinase family. The observed interaction suggests that the asparagine of this motif helps to align the phosphate groups of the nucleotide for the phosphorylation reaction. Interestingly, O2B of the β-phosphate group forms a dative bond with a magnesium ion (Figure 4). The assignment of a magnesium ion instead of a water molecule at this position is strongly supported by the quasi-octahedral coordination geometry exhibited by the side chain carboxylate groups of Asp184 at the C-terminus of β9 and Glu205 at the N-terminus of α7, AMP·PN, GMB (in protomer B), and several water molecules in this region. Studies on ribokinases and adenosine kinases from different species, which belong to the PfkB carbohydrate kinase family as well, have shown that divalent cations (presumably a magnesium ion in vivo) are required for catalysis. Moreover, mutagenesis studies on some other members of this family have shown that the glutamate of the NXXE motif, which corresponds to Glu205 in HldA, is important for the binding of a magnesium ion in the active site.[28] The γ-phosphate group of AMP·PNP could not be located in either protomer because of the lack of electron densities.

In contrast to the nucleotide-binding site, the heptose-binding site in each protomer is constituted by residues from both the α/β core and the protruding twisted β-sheet and by two residues from the loop connecting β2 to β3 of the opposite protomer. Importantly, in protomer A, the γ-carboxylate group of Asp270A forms a hydrogen bond with the 1-hydroxyl group of M7P. The η-hydroxyl group of Tyr159 forms a hydrogen bond with the 1-hydroxyl group of M7P as well in protomer A and with the phosphoester oxygen atom at position 1 of GMB in protomer B. In both protomers, the 2-hydroxyl group of the heptose forms hydrogen bonds with the main-chain NH group of Gly59 at the C-terminus of β3, the η-hydroxyl group of Tyr159 and the γ-carboxylate group of Asp270. The 3-hydroxyl group of the heptose forms hydrogen bonds with the γ-carboxylate group of Asp29 in β2 and the main-chain NH group of Gly59, while the 4-hydroxyl group of the heptose forms hydrogen bonds with the γ-carboxylate group of Asp29 and the ζ-guanidinium group of Arg115, the latter of which is positioned by the δ-carboxylate group of Glu42 of the opposite protomer through an ionic interaction. The 6-hydroxyl group of the heptose forms hydrogen bonds with the ζ-guanidinium group of Arg125, which is positioned by the side chain carboxylate groups of Asp127 of the parent protomer and Glu42 of the opposite protomer through ionic interactions. Importantly, the ζ-guanidinium group of Arg125, together with the ε-amine groups of Lys113 at the N-terminus of β6, Lys161 in the loop connecting β8 to α5, and Lys186 in the loop connecting β9 to α6 of the parent protomer, and with the ζ-guanidinium group of Arg38 of the opposite protomer, also forms ionic interactions with the 7-phosphate group of the heptose (Figure 5). This partly accounts for the specificity of HldA for M7P. Through ionic interactions, the ε-amine group of Lys113 is positioned by the side chain carboxylate groups of Asp127 and Glu129; the ε-amine group of Lys161 is positioned by the δ-carboxylate group of Glu129, and the ε-amine group of Lys186 is positioned by the side chain carboxylate groups of Asp184 and Glu205. In protomer B, the 1-phosphate group of GMB was assigned half occupancy during structural model refinement because its less well-defined electron densities suggest that only a limited amount of M7P had been phosphorylated. No significant structural or conformational differences were observed between the two protomers that could account for the binding of M7P in protomer A and GMB in protomer B. Examination of crystal packing did not reveal any relevance with this mode of binding either.

Interestingly, in protomer A, two water molecules were located between the β-phosphate group of AMP·PN and the 1-hydroxyl group of M7P. It is possible that the electron densities of these two water molecules actually belong to two of the oxygen atoms

dx.doi.org/10.1021/jm301483h | J. Med. Chem. 2013, 56, 1405−1417

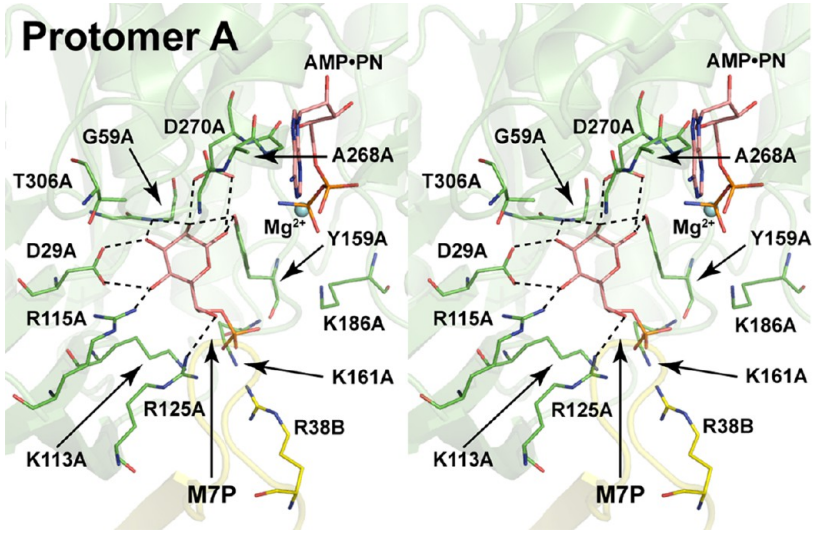

Figure 5. Heptose-binding site. Only the site in protomer A is shown, as the heptose-binding interactions in protomer B are essentially the same. AMP·PN, M7P, and all of the residues involved are shown with stick models, while the magnesium ion is shown in cyan. For clarity, only some of the residues are labeled. All of the hydrogen bonds involved are indicated by dashed lines.

of the dynamically disordered γ-phosphate group of AMP·PNP. On the basis of the positions of these two water molecules, the γ-phosphate group was modeled. The phosphorus atom of the γ-phosphate group of AMP·PNP and the oxygen atom of the 1-hydroxyl group of M7P are aligned head-on at a distance of 3.1 Å (Figure 6A). In protomer B, the 1-phosphate group of GMB forms hydrogen bonds through OP1 with the main-chain NH groups of Gly269B and Asp270B and through OP2 with the main-chain NH group of Gly267. OP3 forms a dative bond with the magnesium ion. The distance between N3B of the β-phosphate group of AMP·PN and the phosphorus atom of the 1-phosphate group of GMB is 4.8 Å (Figure 6B). These observations together strongly indicate the feasibility of an in-line mechanism, which has been proposed for other members of the PfkB carbohydrate kinase family, being adopted by the HldA-catalyzed phosphorylation. Asp270 of the GXGD signature motif acts as a catalytic base, with its γ-carboxylate group deprotonating the 1-hydroxyl group of M7P. The deprotonatation of the 1-hydroxyl group of M7P favors its oxygen atom performing a nucleophilic attack at the phosphorus atom of the γ-phosphate group of ATP. The GXGD signature motif forms an anion hole at the N-terminus of α9, in which the positive end of the helix dipole of α9 and the hydrogen bonds donated by the main-chain NH groups of the GXGD signature motif, together with the magnesium ion, help to accommodate the additional negative charge in the γ-phosphate group of ATP during the nucleophilic attack, thereby lowering the energy of the transition state. The nucleophilic attack results in the formation of a phosphoester bond between the 1-hydroxyl group of M7P and the γ-phosphate group of ATP and in the dissociation of the phosphodiester bond between the β- and the γ-phosphate groups of ATP, thereby producing GMB and ADP (Figure 6C).

Mutagenesis Studies on the in Vivo Activity of HldA. A plasmid encoding the wild-type HldA (pSL3) has been tested previously for its ability to complement the LPS phenotype of a *B. cenocepacia* Δ*hldA* mutant strain (RSF39). Upon gel electrophoresis and silver staining, LPS extracted from the parental strain exhibited a ladder-like appearance, indicating the presence of lipid A, complete core OS, and an O-antigen polysaccharide chain with a variable number of saccharide units. RSF39 conjugated with the vector control pSCrhaB2 produced LPS with a truncated (heptoseless) core OS, which migrated as a single band of low molecular weight. In contrast, pSL3 restored in RSF39 the LPS phenotype of the parental strain.[29] On the basis of the structure of HldA ES/EP, seven residues were selected for an assessment of their importance in the in vivo activity of HldA using this method. A plasmid encoding HldA Y159F restored the parental LPS phenotype in RSF39, whereas one encoding HldA D270A showed an LPS profile similar to that of RSF39 carrying the vector control pSCrhaB2. These data support the conclusion that the catalytic residue of HldA is Asp270, not Tyr159. The heptose-binding site of each protomer involves Glu42 of the opposite protomer. A plasmid encoding the E42A variant partially restored the parental LPS phenotype in RSF39, indicating that Glu42 is not absolutely required for the in vivo activity of HldA. This is consistent with the apparent lack of direct participation of Glu42 in the catalytic mechanism of HldA. However, a significant amount of LPS extracted from the conjugated RSF39 consisted of lipid A and a truncated core OS, indicating that Glu42 is a significant contributor to the in vivo activity of HldA. This can be explained by the importance of Glu42 in the formation of a catalytically favorable heptose-binding site: Glu42 of each protomer positions Arg115 and Arg125 of the opposite protomer for interacting with the 4-hydroxyl, the 6-hydroxyl, and the 7-phosphate groups of M7P. These interactions in turn help to position M7P for phosphorylation. Results of the mutagenesis studies did not reflect the importance of Asp184, Lys186, Asn202, and Glu205 suggested by the structure of HldA ES/EP. Plasmids encoding the D184A, the K186A, the N202A, and the E205A variants restored the parental LPS phenotype in RSF39 similarly as pSL3 did. Possibly, the functional effects of these substitutions are not significant in vivo or are diminished by other residues in proximity (Figure 7).

Identification of HldA Inhibitors. We have identified quercetin, piceatannol, and several compounds in the tyrphostin family as HldA inhibitors in a previous screen (unpublished results). These compounds are broad-spectrum kinase inhibitors lacking the selectivity required for serving as leads in drug development. Inhibitors **1** and **2** were optimized using medicinal chemistry from a high-throughput screening hit discovered at MUTABILIS against the N-terminal kinase domain of *E.coli*

dx.doi.org/10.1021/jm301483h | *J. Med. Chem.* 2013, 56, 1405−1417

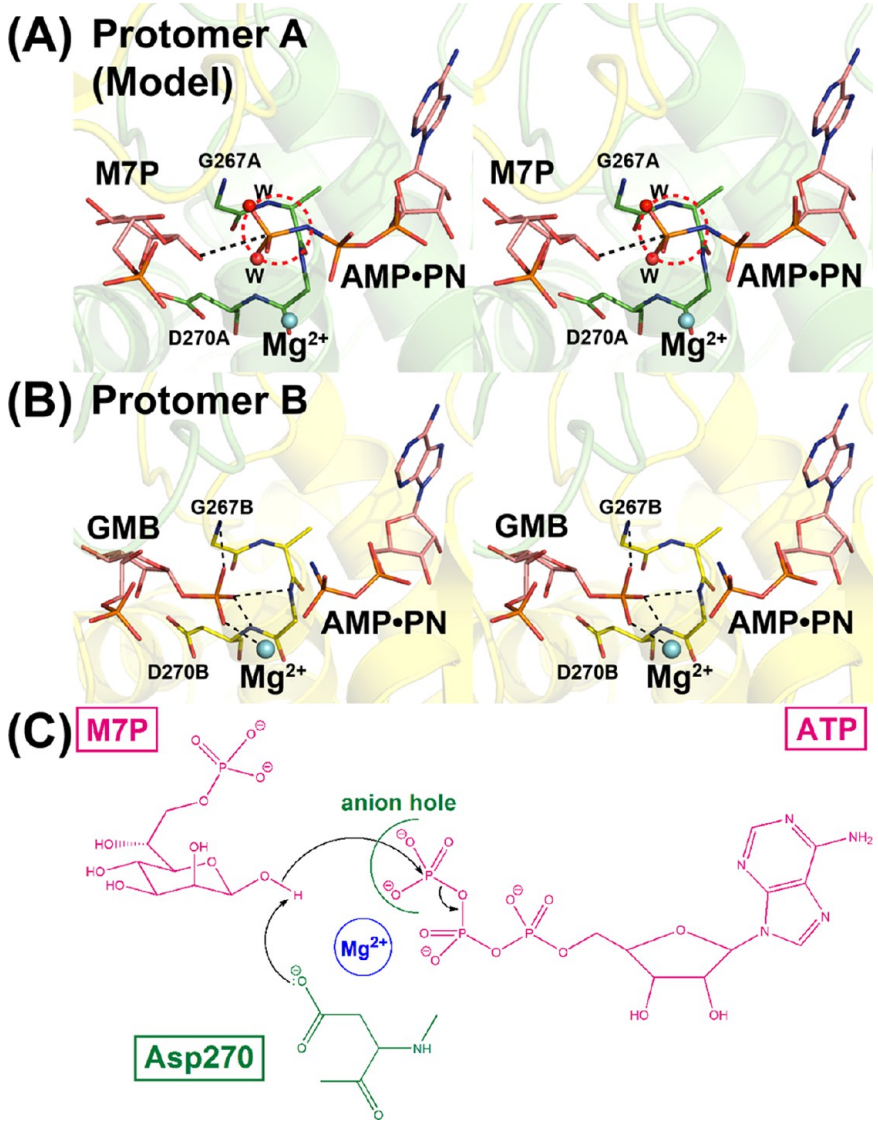

Figure 6. Catalytic mechanism of HldA. (A) On the basis of the positions of the two water molecules (shown in red and labeled W) located between AMP·PN and M7P (both shown with stick models) in protomer A, an additional phosphate group (circled in red) was modeled onto AMP·PN. The head-on alignment of the γ-phosphate group of AMP·PNP with the 1-hydroxyl group of M7P is indicated by a dotted line. Residues of the GXGD signature motif are shown with stick models as well, while the magnesium ion is shown in cyan. (B) In protomer B, the 1-phosphate group of GMB forms hydrogen bonds with the main-chain NH groups of residues of the GXGD signature motif and an ionic interaction with the magnesium ion (all indicated by dashed lines). (C) Proposed catalytic mechanism of HldA.

HldE; that work is reported in the subsequent article, in which inhibitors **1** and **2** are described as compounds **25** and **85**, respectively.[23,24] Inhibitors **1** and **2** were shown to inhibit *B. cenocepacia* HldA at IC_{50} values of 0.81 and 0.23 μM, respectively.

Crystal Structures of His_6-HldA:1, HldA:M7P:1, and HldA:2 (Resolution: 2.60−3.05 Å). The overall structure of HldA is preserved in all of the three HldA−inhibitor complexes. At the initial stage of structural model refinement, outstanding electron densities were found in the nucleotide-binding site of each protomer of these complexes. The shapes and the magnitudes of these electron densities indicate that inhibitor **1** binds in this location of each protomer of His_6-HldA:**1** and HldA:M7P:**1** (Figure 8) while inhibitor **2** binds in this location of each protomer of HldA:**2**. Outstanding electron densities were found in the heptose-binding site of each protomer of HldA:M7P:**1** as well. Those in protomer A were of sufficient quality to justify the assignment of M7P in the β-pyranose form and in the chair conformation (Figure 8), whereas those in protomer B could justify the assignment of only a phosphate ion that corresponds to the 7-phosphate group of M7P.

Both inhibitors **1** and **2** improve their shape complementarity with the nucleotide-binding sites of HldA by adopting a folded conformation, with their phenyltriazine, linker, and benzothiazole moieties roughly corresponding to the adenine, the ribose, and the phosphate moieties of AMP·PN, respectively (Figure 9A). However, compared with AMP·PN, these inhibitors penetrate the nucleotide-binding sites more deeply, thereby enhancing their hydrophobic interactions with the protein, which constitute the majority of HldA−inhibitor interactions (Figure 9B). These inhibitors make van der Waals contacts with the main-chain atoms of Ser240, Glu241, Gly243, Gly269, and Gly298 and with the side chains of Asn202, Thr238, Met244, Ala257, Ala259, Val262, Val265, Ala268, Val272, Ala297, and Val301. Only two hydrogen bonds were observed between these inhibitors and HldA. N3

dx.doi.org/10.1021/jm301483h | J. Med. Chem. 2013, 56, 1405−1417

of the benzothiazole moiety forms a hydrogen bond with the main-chain NH group of Ser240, while the NH group of the linker moiety forms a hydrogen bond with the β-amide group of Asn294. The carboxylate group of the benzothiazole moiety forms a dipole−dipole interaction with the β-amide group of Asn202 (Figure 10). Inhibitor **1** has a methoxyl substituent at phenyl C2 and C6, whereas inhibitor **2** has a chloride substituent at the corresponding positions. Nevertheless, no significant differences were observed between these inhibitors in their interactions with HldA. For both inhibitors, one of the substituents protrudes into the solvent, whereas the other interacts with the benzothiazole moiety in a lipophilic (for methoxyl) or a chloride−π (for chloride) manner (Figure 9A). Importantly, in protomer A of HldA:M7P:**1**, no interactions were observed between inhibitor **1** and M7P, indicating that the binding of either ligand does not favor or disfavor that of the other (Figure 10). This strongly suggests that inhibitors **1** and **2** do not use the exclusion of M7P as a strategy for inhibiting HldA. Kinetic studies showed that these inhibitors are purely ATP-competitive.[24]

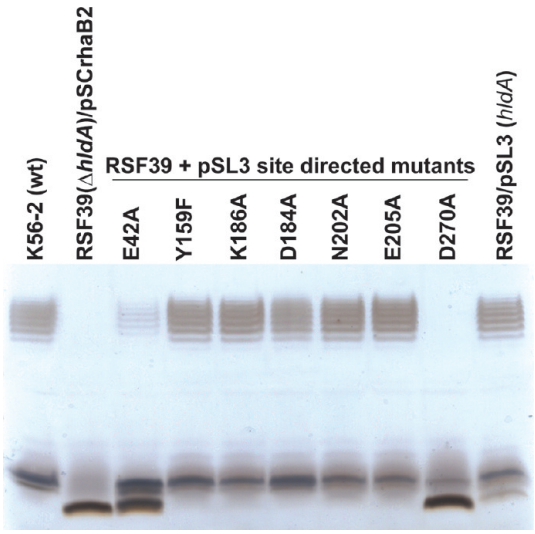

Figure 7. LPS profiles. LPS extracted from the wild-type *B. cenocepacia* strain K56-2 and from the K56-2 Δ*hldA* mutant (RSF39) conjugated with the vector control pSCrhaB2, with plasmids encoding substitutions of the seven selected residues in HldA (pSL3 site-directed mutants), and with a plasmid encoding the wild-type HldA (pSL3) was separated by gel electrophoresis and stained with silver nitrate. Bands with ladder-like appearance near the top of the gel correspond to LPS molecules with lipid A, a complete core OS, and an O-antigen polysaccharide chain with a variable number of saccharide units. Near the bottom of the gel, the band of higher molecular weight (as seen for K56-2) corresponds to LPS molecules with lipid A and a complete core OS, whereas the band of lower molecular weight (as seen for RSF39) corresponds to LPS molecules with lipid A and a truncated (heptoseless) core OS.

The virtually complete reliance of the HldA−inhibitor binding on hydrophobic interactions suggests that the potential of hydrophobic interactions should be fully exploited in the design of new HldA inhibitors. Inhibitors **1** and **2** achieve this by adopting a folded conformation. The shape complementarity could be further improved by adding substituents to some positions of the inhibitor, provided that these substituents would not sterically hinder the folding of the inhibitor or prevent its entry into the nucleotide-binding sites of HldA. On the other hand, the potential of hydrogen-bonding and ionic interactions is evident in HldA ES/EP. For example, the linker and the benzothiazole moieties of the inhibitor could be redesigned to interact with residues of HldA that form hydrogen bonds with AMP·PN in HldA ES/EP.

CONCLUSION

HldA functions as a homodimeric enzyme in which each protomer comprises an α/β core providing the platform for catalytic

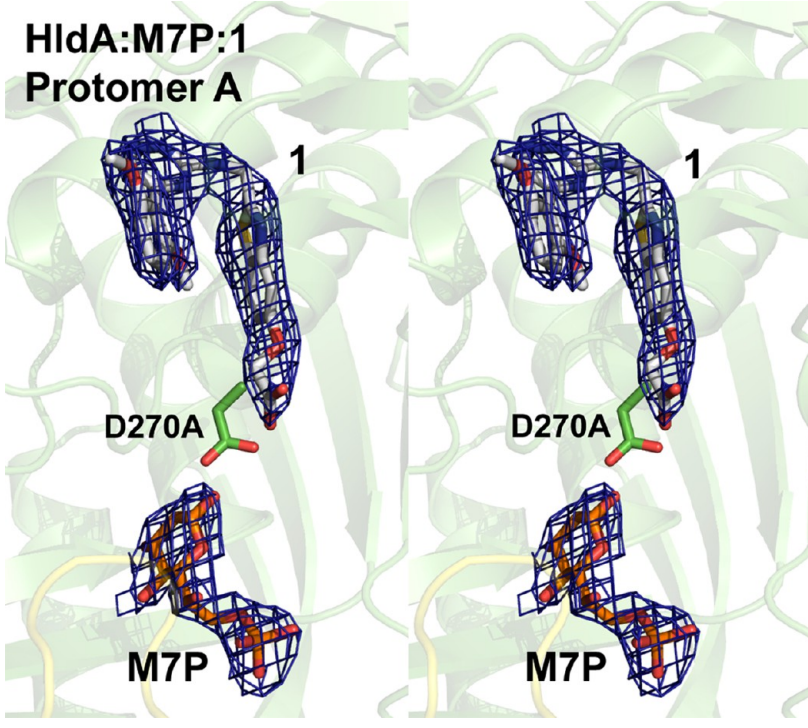

Figure 8. Residual electron densities in the $(2|F_o| - |F_c|)\alpha_c$ maps of HldA:M7P:**1** (protomer A) contoured at 1.0σ. Electron densities associated with the inhibitors were observed in protomer B of HldA:M7P:**1** and both protomers of His_6-HldA:**1** and HldA:**2** as well. Asp270, M7P, and inhibitor **1** are shown with stick models.

dx.doi.org/10.1021/jm301483h | J. Med. Chem. 2013, 56, 1405−1417

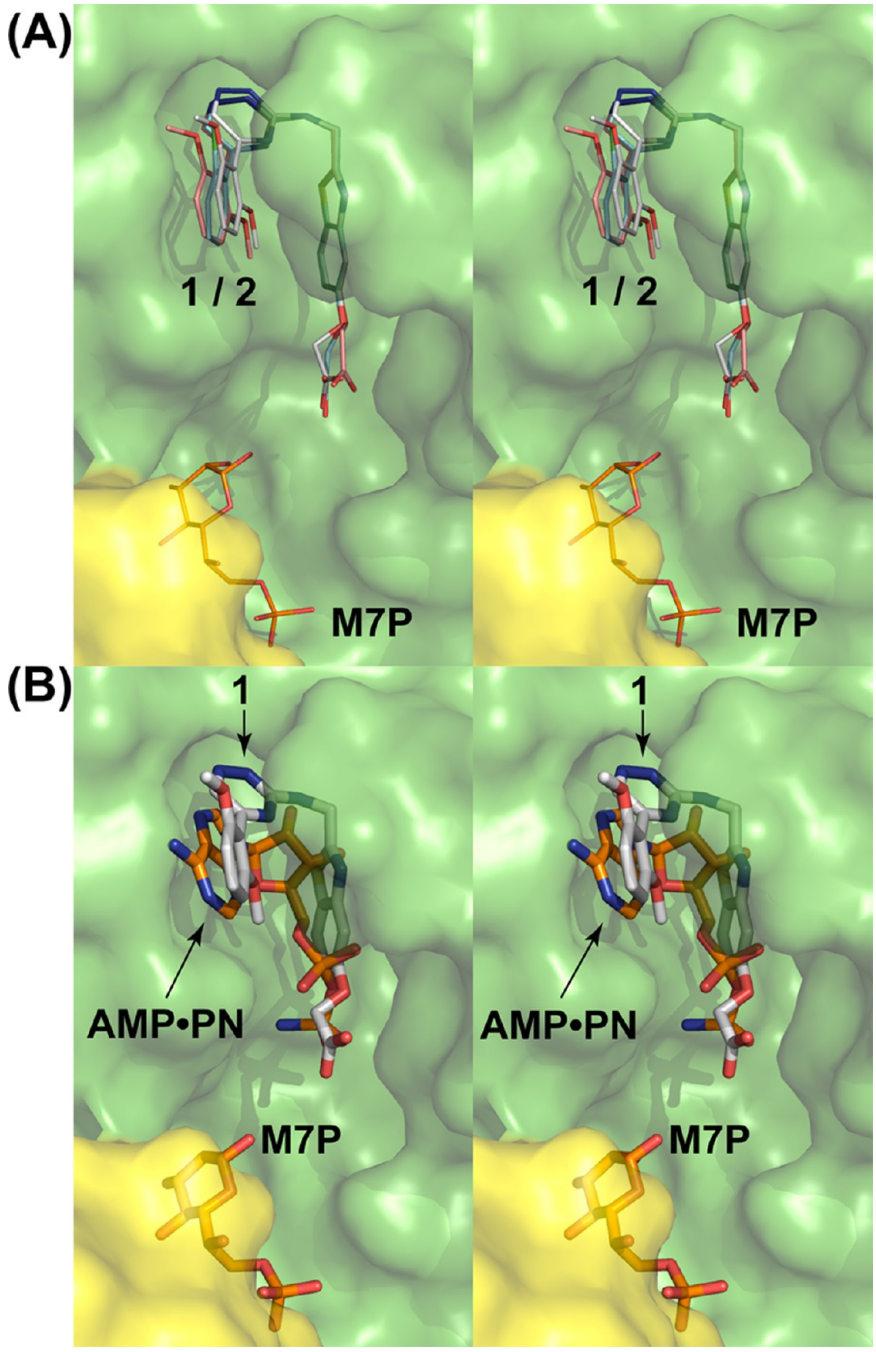

Figure 9. Comparisons among the inhibitors and AMP·PN in the nucleotide-binding site of HldA. (A) Inhibitor **1** (shown with pink and white stick models, as observed in protomer B of His_6-HldA:**1** and protomer A of HldA:M7P:**1**, respectively) versus inhibitor **2** (shown with a cyan stick model, as observed in protomer A of HldA:**2**). (B) Inhibitor **1** (shown with a white stick model, as observed in protomer A of HldA:M7P:**1**) versus AMP·PN (shown with a gold stick model, as observed in protomer A of HldA ES/EP). The protein surface was calculated and M7P was shown based on the structure of HldA:M7P:**1**.

activity and a protruding twisted β-sheet mainly involved in dimerization. The nucleotide-binding interactions and the heptose-binding interactions of HldA share similar properties with their respective counterparts in other proteins. The adenine ring of the nucleotide forms hydrophobic interactions with HldA, while the ribose ring and the phosphate groups of the nucleotide interact with HldA mainly through hydrogen bonding. Heptose binding is mediated mainly by hydrogen bonding as well in HldA. In addition, several positively charged residues, which are positioned by several negatively charged residues of the same and the opposite protomers through a network of ionic interactions, contribute to the specificity of HldA for M7P. Apparently, the HldA-catalyzed phosphorylation adopts the in-line mechanism proposed for other members of the PfkB carbohydrate kinase family as well, in which the transition state is stabilized by a magnesium ion, the anion hole (formed by the GXGD signature motif), and the helix dipole of α9 of HldA. Results of the mutagenesis studies on the in vivo activity of HldA confirm the role of the conserved aspartate, Asp270, as the catalytic residue.

Both inhibitors **1** and **2** bind to the nucleotide-binding sites of HldA without altering the overall structure of the enzyme or interfering with the binding of M7P. Both inhibitors adopt a

dx.doi.org/10.1021/jm301483h | *J. Med. Chem.* 2013, 56, 1405−1417

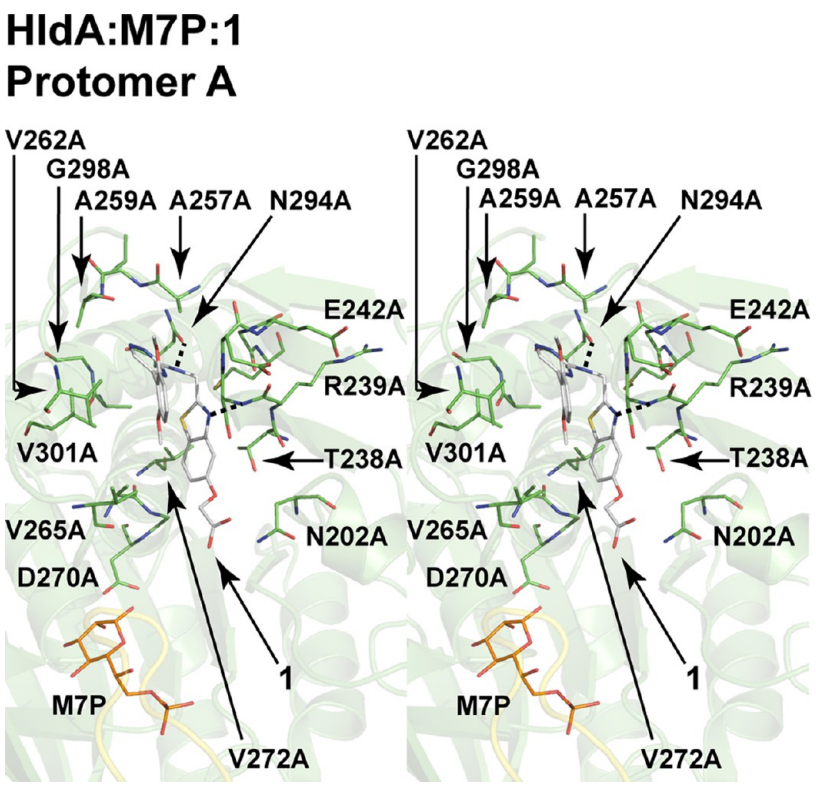

Figure 10. HldA–inhibitor interactions. Only the nucleotide-binding site in protomer A of HldA:M7P:**1** is shown, as the inhibitor-binding interactions are essentially the same in protomer B of HldA:M7P:**1** and both protomers of His_6-HldA:**1** and HldA:**2**. Inhibitor **1**, M7P, and all of the residues involved are shown with stick models. For clarity, only some of the residues are labeled. All of the hydrogen bonds involved are indicated by dotted lines.

folded conformation to improve their shape complementarity with the nucleotide-binding sites of HldA and penetrate the sites more deeply than AMP·PN does to enhance their hydrophobic interactions with the enzyme. The HldA–inhibitor interactions are mainly hydrophobic in nature with limited contribution by hydrogen bonding and dipole–dipole interaction. The structures of the HldA–inhibitor complexes provide clues for rational modification of the inhibitors.

Urged by the rapid evolution of MDR, research in bacterial physiology has been very active in identifying targets for new antibacterial therapeutics.[3] Interest has been growing in LPS biosynthesis as a target for the development of antivirulence drugs and antibiotic adjuvants against Gram-negative bacteria. In particular, the biosynthetic pathway of ADP-L-glycero-β-D-manno-heptose, the precursor for LPS biosynthesis, has recently been gaining attention from the pharmaceutical sector.[2,23,24,30,31] This work provides essential structural–functional information of HldA, an important enzyme in the biosynthetic pathway of ADP-L-glycero-β-D-manno-heptose, and valuable insight into its catalytic mechanism, thereby supporting medicinal chemists in their design of new HldA inhibitors. In view of the general concern about the lack of selectivity of inhibitors targeting nucleotide-binding sites, it is expected that future attention will be drawn to the pursuit of inhibitors targeting the heptose-binding sites of HldA. Design of bivalent inhibitors targeting both the nucleotide- and the heptose-binding sites of HldA presents an exciting prospect in the long run as well. Furthermore, most Gram-negative bacterial species employ HldE instead of HldA and HldC in the biosynthesis of ADP-L-glycero-β-D-manno-heptose. However, studies of HldE have been hindered by the lack of structural information. Crystallization of HldE has been a major challenge probably because of the dynamic behaviors of this two-domain protein. Because of the homology of HldA with the N-terminal domain of HldE, this work will be of great importance for our understanding of HldE and the design of new HldE inhibitors as well.

EXPERIMENTAL SECTION

General. All chemicals, unless otherwise specified, were purchased from various commercial sources and used without further purification. M7P was synthesized in-house as previously described.[32] The synthesis of inhibitors **1** and **2** is reported in the Supporting Information of the subsequent article (therein described as compounds **25** and **85**, respectively).[24] Both inhibitors display HPLC purity of >95% and have been characterized by ^{1}H NMR, MS, and crystallographic data.

Expression and Purification of HldA. *B. cenocepacia hldA* gene was cloned into the Gateway pDEST17 vector using the Gateway cloning system (Invitrogen). Chemically competent cells of the *E. coli* strain BL21(DE3)-T1^R (Sigma) were transformed with pDEST17-*hldA*, liquid-cultured to an optical density of 0.5 at a wavelength of 600 nm, and induced with 1 mM isopropyl β-D-1-thiogalactopyranoside for 4 h. Cells were harvested by centrifugation at 2392*g* for 20 min and resuspended in the lysis buffer (50 mM Tris, pH 8.0, 40 mM imidazole, 2.8 mM 2-mercaptoethanol, and 500 mM potassium chloride) with peptidase inhibitors added (2 μM leupeptin, 2 μM pepstatin A, and 2 mM benzamidine hydrochloride). Resuspended cells were lysed using the French press method at a pressure of 1000 psi for 4 times. The lysate was centrifuged at 33152*g* for 40 min. The supernatant was filtered with Pall Metricel membranes with a pore size of 0.45 μm and loaded onto a HiTrap chelating HP column (GE Healthcare) precharged with 100 mM nickel chloride and pre-equilibrated with the lysis buffer. The column was washed with 30 mM imidazole in the lysis buffer, and elution was with 600 mM imidazole in the lysis buffer, using the ÄKTA fast protein liquid chromatography system (GE Healthcare). The eluate was passed through a HiPrep 26/10 desalting column (GE Healthcare) pre-equilibrated with either the crystallization buffer (10 mM Tris, pH 7.5, 170 mM potassium chloride, and 1 mM EDTA, if His_6-HldA was the desired final product) or the proteolysis buffer (50 mM Tris, pH 8.0,

dx.doi.org/10.1021/jm301483h | J. Med. Chem. 2013, 56, 1405–1417

100 mM potassium chloride, and 500 μM EDTA, if HldA was the desired final product). To yield HldA, the hexahistidine affinity tag of His_6-HldA was removed by incubation at 25 °C for 3 h, with 200 μg of tobacco etch virus peptidase added. The released hexahistidine affinity tag and any other impurities were eliminated by passing the reaction mixture through the desalting and the chelating columns, both pre-equilibrated with the lysis buffer. The flow-through was passed through the desalting column pre-equilibrated with the crystallization buffer.

X-ray Crystallography. All of the crystals were grown by the hanging-drop vapor diffusion method. Crystals of HldA ES/EP were grown at 20 °C for several months. The drop contained 1 μL of the protein solution (0.7 mg/mL HldA, 2.5 mM Tris, pH 7.5, 42.5 mM potassium chloride, 0.25 mM EDTA, 1 mM M7P, 1 mM AMP·PNP, 5 mM magnesium chloride, and 30% 1,6-hexanediol) and 1 μL of the precipitant solution (condition no. 27 of Hampton Research Crystal Screen, 0.2 M sodium citrate, 0.1 M HEPES, pH 7.5, and 20% v/v 2-propanol), while the reservoir contained 500 μL of 1.4 M ammonium sulfate. Crystals of His_6-HldA:**1** were grown at 4 °C for 1 month. The drop contained 1 μL of the protein solution (5.0 mg/mL His_6-HldA, 10 mM Tris, pH 7.5, 170 mM potassium chloride, 1 mM EDTA, 150 μM M7P, and 500 μM inhibitor **1**) and 1 μL of the precipitant solution (50 mM HEPES, pH 7.5, 0.05% w/v polyethylene glycol, M_r = 400, and 0.5 M ammonium sulfate), while the reservoir contained 500 μL of 1 M ammonium sulfate. Crystals of HldA:M7P:**1** were grown at 4 °C for 1 month. The drop contained 1 μL of the protein solution (5.0 mg/mL HldA, 10 mM Tris, pH 7.5, 170 mM potassium chloride, 1 mM EDTA, 150 μM M7P, and 500 μM inhibitor **1**) and 1 μL of the precipitant solution (0.1 M HEPES, pH 7.5, 10% w/v polyethylene glycol, M_r = 10 000, and 4% v/v ethylene glycol), while the reservoir contained 500 μL of 1 M ammonium sulfate. Crystals of HldA:**2** were grown in the same conditions as those of His_6-HldA:**1** except that HldA and inhibitor **2** were used instead of His_6-HldA and inhibitor **1**, respectively. For cryoprotection, all of the crystals were kept at 4 °C with the reservoir changed to 500 μL of 2 M ammonium sulfate for several days before flash-cooling. All of the X-ray diffraction data were collected at the National Synchrotron Light Source at Brookhaven National Laboratory. All of the data sets were indexed, scaled, and merged using HKL-2000.[33] Initial phases were obtained for HldA ES/EP by the single-wavelength anomalous dispersion method, and for His_6-HldA:**1**, HldA:M7P:**1**, and HldA:**2** they were obtained by the molecular replacement method using the structure of HldA ES/EP as the search model. Structural models were built and refined using PHENIX and were manually adjusted when needed during refinement using Coot.[34,35] The stereochemical quality, the topology, and the interactions (protein−protein, protein−ligand, and protein−metal ion) within each structural model were analyzed using PDBsum.[36] Solvent-accessible surface areas were calculated using AREA-IMOL.[37−39] Graphical representations of the structural models were prepared using PyMOL.[40]

LPS Production Assay. The cloning vector pSCrhaB2, a plasmid encoding the wild-type HldA (pSL3), and pSL3 derivatives encoding substitutions of the seven selected residues were transferred to a *B. cenocepacia* strain K56-2 Δ*hldA* mutant (RSF39) by triparental conjugation.[17,29,41] Exoconjugants were selected for on LB-agar plates containing 100 μg/mL trimethoprim and 50 μg/mL gentamicin. Plasmid transfer was confirmed by PCR. Exoconjugants were grown overnight on LB-agar plates containing 100 μg/mL trimethoprim, with gene expression induced by 0.2% rhamnose. LPS was extracted from the cells, separated by gel electrophoresis, and stained with silver nitrate as previously described.[17,42,43]

HldA Inhibition Assay. This assay was based on the detection of ATP depletion by luciferase. All chemicals, except M7P and the inhibitors, were purchased from Sigma. The assay buffer (AB) consisted of 50 mM HEPES, pH 7.5, 1 mM manganese(II) chloride, 25 mM potassium chloride, 0.012% Triton-X100, 0.1 μM myelin basic protein, and 1 mM DTT. The inhibitor being examined was dissolved at different concentrations in DMSO/water or DMSO only. Then 3 μL of each inhibitor solution and 28 μL of HldA in AB were mixed in each well of a white polystyrene Costar plate. After preincubation at room temperature for 30 min, 29 μL of the substrate mixture (ATP and M7P in AB) was added to each well to give a total volume of 60 μL. The reaction mixtures had 50 nM HldA, 0.2 μM M7P, 0.2 μM ATP, and different concentrations of the inhibitor being examined in AB. After incubation at room temperature for 30 min, an amount of 200 μL of the revelation mixture (luciferase, D-luciferin and *N*-acetylcysteamine) was added to give a total volume of 260 μL containing 30 nM luciferase, 30 μM D-luciferin, and 100 μM *N*-acetylcysteamine. Luminescence intensity was measured on a Luminoskan reader (Thermofisher). Values of percentage inhibition were fitted to a classical equilibrium model with the Hill coefficient, n_H, using XLFIT (IDBS):

$$\%\ \text{inhibition} = 100 \times ([\text{inhibitor}])^{n_H}/([\text{inhibitor}]^{n_H} + IC_{50}{}^{n_H})$$

■ ASSOCIATED CONTENT

Ⓢ Supporting Information

Quality of the crystal structures, structural relationship of HldA with other members of the PfkB carbohydrate kinase family, nucleotide-binding sites of HldA, heptose-binding sites of HldA, potassium-binding sites of HldA, and binding of inhibitors **1** and **2** to HldA. This material is available free of charge via the Internet at http://pubs.acs.org.

Accession Codes

The following structures are listed with their PDB codes in parentheses: HldA ES/EP (4E84), His_6-HldA:**1** (4E8W), HldA:M7P:**1** (4E8Y), HldA:**2** (4E8Z).

■ AUTHOR INFORMATION

Corresponding Author

*Phone: 905-525-9140, extension 22912. Fax: 905-522-9033. E-mail: junopm@mcmaster.ca.

Present Addresses

[∞]Galapagos SASU, 102 Avenue Gaston Roussel, 93230 Romainville, France.

[×]GlaxoSmithKline, 25-27 Avenue du Québec, 91951 Les Ulis, France.

[●]Department of Microbiology and Immunology, University of British Columbia, Vancouver, British Columbia, V6T 1Z4, Canada.

Author Contributions

[#]These authors contributed equally to this work.

Notes

The authors declare no competing financial interest.

■ ACKNOWLEDGMENTS

All X-ray diffraction data used in this study were collected at beamline X25 of the National Synchrotron Light Source. Funding for NSLS comes primarily from the Offices of Biological and Environmental Research and of Basic Energy Sciences of the U.S. Department of Energy and from the National Center for Research Resources (Grant P41RR012408) and the National Institute of General Medical Sciences (Grant P41GM103473) of the National Institutes of Health. T.-W.L. received a postdoctoral fellowship from the Ontario Ministry of Research and Innovation. This work was supported by Canadian Institutes of Health Research Operating Grant XNE-8705 to M.A.V. and M.S.J., a grant from Cystic Fibrosis Canada to M.A.V., and a grant from the Austrian Science Fund FWF (Grant P 22909) to P.K. M.A.V. holds a Canada Research Chair in Infectious Diseases and Microbial Pathogenesis.

■ ABBREVIATIONS USED

MDR, multidrug resistance; LPS, lipopolysaccharide; OS, core oligosaccharide; KDO, 2-keto-3-deoxy-D-manno-octosonic acid;

M7P, D-glycero-β-D-manno-heptose 7-phosphate; GMB, D-glycero-β-D-manno-heptose 1,7-bisphosphate; ES, enzyme−substrate complex; EP, enzyme−product complex; rmsd, root-mean-square deviation; AB, assay buffer

REFERENCES

(1) Nikaido, H. Multidrug resistance in bacteria. *Annu. Rev. Biochem.* **2009**, *78*, 119−146.

(2) Wright, G. D.; Sutherland, A. D. New strategies for combating multidrug-resistant bacteria. *Trends Mol. Med.* **2007**, *13*, 260−267.

(3) Brown, E. D.; Wright, G. D. New targets and screening approaches in antimicrobial drug discovery. *Chem. Rev.* **2005**, *105*, 759−774.

(4) Bugg, T. D. H.; Braddick, D.; Dowson, C. G.; Roper, D. I. Bacterial cell wall assembly: still an attractive antibacterial target. *Trends Biotechnol.* **2011**, *29*, 167−173.

(5) Schweizer, H. P. Understanding efflux in Gram-negative bacteria: opportunities for drug discovery. *Expert Opin. Drug Discovery* **2012**, *7*, 633−642.

(6) Oblak, M.; Kotnik, M.; Solmajer, T. Discovery and development of ATPase inhibitors of DNA gyrase as antibacterial agents. *Curr. Med. Chem.* **2007**, *14*, 2033−2047.

(7) Geoffroy, M.-C.; Floquet, S.; Métais, A.; Nassif, X.; Pelicic, V. Large-scale analysis of the meningococcus genome by gene disruption: resistance to complement-mediated lysis. *Genome Res.* **2003**, *13*, 391−398.

(8) Vaara, M. Outer membrane permeability barrier to azithromycin, clarithromycin, and roxithromycin in Gram-negative enteric bacteria. *Antimicrob. Agents Chemother.* **1993**, *37*, 354−356.

(9) Nikaido, H. Molecular basis of bacterial outer membrane permeability. *Microbiol. Rev.* **1985**, *49*, 1−32.

(10) Nikaido, H. Molecular basis of bacterial outer membrane permeability revisited. *Microbiol. Mol. Biol. Rev.* **2003**, *67*, 593−656.

(11) Raetz, C. R. H.; Whitfield, C. Lipopolysaccharide endotoxins. *Annu. Rev. Biochem.* **2002**, *71*, 635−700.

(12) Barb, A. W.; Zhou, P. Mechanism and inhibition of LpxC: an essential zinc-dependent deacetylase of bacterial lipid A synthesis. *Curr. Pharm. Biotechnol.* **2011**, *9*, 9−15.

(13) Cipolla, L.; Polissi, A.; Airoldi, C.; Gabrielli, L.; Merlo, S.; Nicotra, F. New targets for antibacterial design: Kdo biosynthesis and LPS machinery transport to the cell surface. *Curr. Med. Chem.* **2011**, *18*, 830−852.

(14) Kneidinger, B.; Marolda, C.; Graninger, M.; Zamyatina, A.; Mcarthur, F.; Kosma, P.; Valvano, M. A.; Messner, P. Biosynthesis pathway of ADP-L-glycero-β-D-manno-heptose in *Escherichia coli*. *J. Bacteriol.* **2002**, *184*, 363−369.

(15) Valvano, M. A.; Messner, P.; Kosma, P. Novel pathways for biosynthesis of nucleotide-activated glycero-manno-heptose precursors of bacterial glycoproteins and cell surface polysaccharides. *Microbiology* **2002**, *148*, 1979−1989.

(16) McArthur, F.; Andersson, C. E.; Loutet, S.; Mowbray, S. L.; Valvano, M. A. Functional analysis of the glycero-manno-heptose 7-phosphate kinase domain from the bifunctional HldE protein, which is involved in ADP-L-glycero-D-manno-heptose biosynthesis. *J. Bacteriol.* **2005**, *187*, 5292−5300.

(17) Loutet, S. A.; Flannagan, R. S.; Kooi, C.; Sokol, P. A.; Valvano, M. A. A complete lipopolysaccharide inner core oligosaccharide is required for resistance of *Burkholderia cenocepacia* to antimicrobial peptides and bacterial survival in vivo. *J. Bacteriol.* **2006**, *188*, 2073−2080.

(18) Taylor, P. L.; Blakely, K. M.; De Leon, G. P.; Walker, J. R.; McArthur, F.; Evdokimova, E.; Zhang, K.; Valvano, M. A.; Wright, G. D.; Junop, M. S. Structure and function of sedoheptulose-7-phosphate isomerase, a critical enzyme for lipopolysaccharide biosynthesis and a target for antibiotic adjuvants. *J. Biol. Chem.* **2008**, *283*, 2835−2845.

(19) Harmer, N. J. The structure of sedoheptulose-7-phosphate isomerase from *Burkholderia pseudomallei* reveals a zinc binding site at the heart of the active site. *J. Mol. Biol.* **2010**, *400*, 379−392.

(20) Taylor, P. L.; Sugiman-Marangos, S.; Zhang, K.; Valvano, M. A.; Wright, G. D.; Junop, M. S. Structural and kinetic characterization of the LPS biosynthetic enzyme D-alpha,beta-D-heptose-1,7-bisphosphate phosphatase (GmhB) from *Escherichia coli*. *Biochemistry* **2010**, *49*, 1033−1041.

(21) Nguyen, H. H.; Wang, L.; Huang, H.; Peisach, E.; Dunaway-Mariano, D.; Allen, K. N. Structural determinants of substrate recognition in the HAD superfamily member D-glycero-D-manno-heptose-1,7-bisphosphate phosphatase (GmhB). *Biochemistry* **2010**, *49*, 1082−1092.

(22) Deacon, A. M.; Ni, Y. S.; Coleman, W. G.; Ealick, S. E. The crystal structure of ADP-L-glycero-D-mannoheptose 6-epimerase: catalysis with a twist. *Structure* **2000**, *8*, 453−462.

(23) Desroy, N.; Moreau, F.; Briet, S.; Le Fralliec, G.; Floquet, S.; Durant, L.; Vongsouthi, V.; Gerusz, V.; Denis, A.; Escaich, S. Towards Gram-negative antivirulence drugs: new inhibitors of HldE kinase. *Bioorg. Med. Chem.* **2009**, *17*, 1276−1289.

(24) Desroy, N.; Denis, A.; Oliveira, C.; Atamanyuk, D.; Briet, S.; Faivre, F.; LeFralliec, G.; Bonvin, Y.; Oxoby, M.; Escaich, S.; Floquet, S.; Drocourt, E.; Vongsouthi, V.; Durant, L.; Moreau, F.; Verhey, T. B.; Lee, T.-W.; Junop, M. S.; Gerusz, V. Novel HldE-K inhibitors leading to attenuated Gram-negative bacterial virulence. Manuscript submitted.

(25) Bork, P.; Sander, C.; Valencia, A. Convergent evolution of similar enzymatic function on different protein folds: the hexokinase, ribokinase, and galactokinase families of sugar kinases. *Protein Sci.* **1993**, *2*, 31−40.

(26) Holm, L.; Rosenström, P. Dali server: conservation mapping in 3D. *Nucleic Acids Res.* **2010**, *38*, W545−W549.

(27) Sigrell, J. A.; Cameron, A. D.; Jones, T. A.; Mowbray, S. L. Structure of *Escherichia coli* ribokinase in complex with ribose and dinucleotide determined to 1.8 Å resolution: insights into a new family of kinase structures. *Structure* **1998**, *6*, 183−193.

(28) Park, J.; Gupta, R. S. Adenosine kinase and ribokinase—the RK family of proteins. *Cell. Mol. Life Sci.* **2008**, *65*, 2875−2896.

(29) Flannagan, R. S.; Linn, T.; Valvano, M. A. A system for the construction of targeted unmarked gene deletions in the genus *Burkholderia*. *Environ. Microbiol.* **2008**, *10*, 1652−1660.

(30) De Leon, G. P.; Elowe, N. H.; Koteva, K. P.; Valvano, M. A.; Wright, G. D. An in vitro screen of bacterial lipopolysaccharide biosynthetic enzymes identifies an inhibitor of ADP-heptose biosynthesis. *Chem. Biol.* **2006**, *13*, 437−441.

(31) Durka, M.; Tikad, A.; Périon, R.; Bosco, M.; Andaloussi, M.; Floquet, S.; Malacain, E.; Moreau, F.; Oxoby, M.; Gerusz, V.; Vincent, S. P. Systematic synthesis of inhibitors of the two first enzymes of the bacterial heptose biosynthetic pathway: towards antivirulence molecules targeting lipopolysaccharide biosynthesis. *Chem.—Eur. J.* **2011**, *17*, 11305−11313.

(32) Zamyatina, A.; Gronow, S.; Puchberger, M.; Graziani, A.; Hofinger, A.; Kosma, P. Efficient chemical synthesis of both anomers of ADP L-glycero- and D-glycero-D-manno-heptopyranose. *Carbohydr. Res.* **2003**, *338*, 2571−2589.

(33) Otwinowski, Z.; Minor, W. Processing of X-ray diffraction data collected in oscillation mode. *Methods Enzymol.* **1997**, *276A*, 307−326.

(34) Adams, P. D.; Afonine, P. V; Bunkóczi, G.; Chen, V. B.; Davis, I. W.; Echols, N.; Headd, J. J.; Hung, L.-W.; Kapral, G. J.; Grosse-Kunstleve, R. W.; McCoy, A. J.; Moriarty, N. W.; Oeffner, R.; Read, R. J.; Richardson, D. C.; Richardson, J. S.; Terwilliger, T. C.; Zwart, P. H. PHENIX: a comprehensive Python-based system for macromolecular structure solution. *Acta Crystallogr.* **2010**, *D66*, 213−221.

(35) Emsley, P.; Lohkamp, B.; Scott, W. G.; Cowtan, K. Features and development of Coot. *Acta Crystallogr.* **2010**, *D66*, 486−501.

(36) Laskowski, R. A. PDBsum new things. *Nucleic Acids Res.* **2009**, *37*, D355−D359.

(37) Collaborative Computational Project Number 4. The CCP4 suite: programs for protein crystallography. *Acta Crystallogr.* **1994**, *D50*, 760−763.

(38) Lee, B.; Richards, F. M. The interpretation of protein structures: estimation of static accessibility. *J. Mol. Biol.* **1971**, *55*, 379−400.

(39) Saff, E. B.; Kuijlaars, A. B. J. Distributing many points on a sphere. *Math. Intell.* **1997**, *19*, 5−11.

(40) *The PyMOL Molecular Graphics System*, version 1.2r2; Schrodinger, LLC: New York.
(41) Cardona, S. T.; Valvano, M. A. An expression vector containing a rhamnose-inducible promoter provides tightly regulated gene expression in *Burkholderia cenocepacia*. *Plasmid* **2005**, *54*, 219−228.
(42) Hitchcock, P. J.; Brown, T. M. Morphological heterogeneity among Salmonella lipopolysaccharide chemotypes in silver-stained polyacrylamide gels. *J. Bacteriol.* **1983**, *154*, 269−277.
(43) Marolda, C. L.; Feldman, M. F.; Valvano, M. A. Genetic organization of the O7-specific lipopolysaccharide biosynthesis cluster of *Escherichia coli* VW187 (O7:K1). *Microbiology* **1999**, *145*, 2485−2495.